

# An approach to determining the Brinell hardness indentation diameter based on contact position

Li Ma<sup>1, 2</sup>, Samuel Low<sup>1</sup>, John Song<sup>2</sup>

<sup>1</sup> National Institute of Standards and Technology, 100 Bureau Drive, Gaithersburg, MD 20899-8553, USA

<sup>2</sup> Kent State University, Kent, OH 44242, USA

## ABSTRACT

Significant differences in Brinell hardness results have been observed worldwide, largely due to the curved surface at the indentation edge making it difficult to measure its diameter. The indenter/material contact boundary under the test force should be the basis for the Brinell indentation diameter; however, the contact boundary cannot be observed using an optical microscope after the indenter is removed as is required by the test methods. Finite element analysis (FEA) models were used to develop a method to effectively determine the location of the indentation contact boundary after unloading, allowing the indentation diameter to be physically defined and measured.

**Section:** RESEARCH PAPER

**Keywords:** Brinell hardness test; indentation contact radius; Finite Element Analysis (FEA); pile-up/sink-in

**Citation:** Li Ma, Samuel Low, John Song, An approach to determining the Brinell hardness indentation diameter based on contact position, Acta IMEKO, vol. 3, no. 3, article 4, September 2014, identifier: IMEKO-ACTA-03 (2014)-03-04

**Editor:** Paolo Carbone, University of Perugia

**Received** February 5<sup>th</sup>, 2013; **In final form** April 22<sup>nd</sup>, 2014; **Published** September 2014

**Copyright:** © 2014 IMEKO. This is an open-access article distributed under the terms of the Creative Commons Attribution 3.0 License, which permits unrestricted use, distribution, and reproduction in any medium, provided the original author and source are credited

**Funding:** (none reported)

**Corresponding author:** Li Ma, e-mail: li.ma@nist.gov

## 1. INTRODUCTION

Although the Brinell hardness test has been widely used by industry for quality control and acceptance testing of metallic materials and products since it was proposed in 1900 by a Swedish researcher J. A. Brinell [1], significant measurement differences have been continually observed worldwide, even among the national metrology institutes that calibrate test block reference standards. These differences increase as they propagate down to the industrial level. The main cause of this problem is that the edge of the indentation is not a distinct boundary, but is instead a curved surface, from either material piling up (pile-up) or sinking in (sink-in), caused by plastic flow of the material surrounding the ball indenter. This makes it difficult to clearly resolve the edge of the indentation and thus to determine the indentation diameter from optical microscope measurement.

The phenomenon of pile-up or sink-in in the indentation process is known to significantly influence the contact area and indentation contact diameter. Early experimental studies of surface deformation around a spherical indenter found that the amount of pile-up and sink-in was related to the strain-

hardening exponent of the materials [2-3] and these were expressed as functional relationships [4]. From finite element analysis (FEA) simulations, the pile-up/sink-in is found to be related, not only to strain hardening  $n$  [5-6], but also to yield strain (the ratio of yield strength  $Y$  to elastic modulus  $E$ ), indentation ratio (indentation depth  $b$  over indenter radius  $R$ ) [7-8] and contact friction [9-10].

We investigated the Brinell indentation contact diameter using confocal microscope measurements and FEA modelling in our former research [13]. This paper continues our formal research to determine the most appropriate definition of the diameter of a Brinell indentation that also allows its unambiguous measurement in the unloaded condition. FEA models were developed to study the location of contact boundaries at the edges of Brinell hardness indentation cross-sectional profiles. From the FEA models, the location of the contact boundary under load is determined and is then tracked after removing the load. The indentation profile shapes from FEA models were confirmed by examining actual Brinell indentations. From the FEA model parameter study results, we developed a new method to effectively determine the

indentation contact boundary after removing the test force and that can be applied to experimental measurements.

## 2. BRINELL HARDNESS TESTS

Brinell hardness tests were made by a secondary calibration laboratory in accordance with ASTM E10 [14] using a calibration Brinell hardness machine. The nominal Brinell hardness value for the test material was 503 HBW 10/3000. The test material was indented using a standard 10 mm diameter tungsten carbide ball indenter and an applied force of 29.42 kN (3000 kgf). The indentation diameters were measured automatically using an image analysing system by the laboratory with a reported expanded uncertainty of better than  $\pm 3 \mu\text{m}$  with a confidence level of 95%. The Brinell hardness number,  $HBW$ , can be calculated [14] as:

$$HBW = 0.102 \times \frac{2F}{\pi D(D - \sqrt{D^2 - d^2})} \quad (1)$$

where  $F$  is the test force in newton,  $D$  is the diameter of the ball indenter in millimeter, and  $d$  is the measured mean diameter of the indentation in millimeter.

## 3. BRINELL INDENTATION PROFILE MEASUREMENT

In order to determine the actual contact diameter, it was necessary to obtain the cross-sectional profile of the indentation. This was accomplished using a contact stylus profilometer. The instrument's lateral resolution is  $0.125 \mu\text{m}$  and the vertical resolution is  $0.0008 \mu\text{m}$ . The nominal radius of the diamond tip is  $2 \mu\text{m}$ . The instrument's auto-crown function can automatically align the diamond tip on the central point (the bottom or top point of the spherical surface), so that several parallel measurement sections can be determined around this point. At each measurement section, the diamond stylus traces on the surface with a traversing speed of  $0.25 \text{ mm/s}$ . The digitized profiles at different sections are collected for analyses.

## 4. FINITE ELEMENT MODELING

Modeling of the Brinell spherical indentation process was performed using a commercial FEA package. Taking advantage of axis-symmetry of the ball indenter and the test material, only cross sections of the ball and test material were modeled. The ball indenter was modeled as rigid. The mesh of the test material used axi-symmetric, four-node bilinear elements with the minimum element size of the specimen being  $0.2 \mu\text{m}$ , which is close to the lateral resolution from the profilometer indentation profile measurements as described above. The test material was modeled as having isotropic elastic-plastic behavior with power-law hardening of the normal form  $\sigma = K\varepsilon^n$  following the von-Mises yield criterion and associative  $J_2$  flow theory. The linear elastic behavior uses Young's modulus  $E$  and Poisson's ratio  $\nu = 0.3$ . From the FEA modeling, the pile-up/sink-in behavior was systematically studied by adjusting various parameters including the material's strain hardening exponent  $n$  and the ratio of Young's modulus to yield strength  $E/Y$ .

## 5. RESULTS AND DISCUSSION

### 5.1. Indentation edge contact point from FEA modeling

Theoretically, the Brinell hardness value should be the ratio of the indentation force to the surface area of indentation. According to international Brinell hardness test method standards, the surface area of indentation is determined by measuring the diameter  $d$  of the resulting indentation after removal of the indentation force [14-15]. Ideally, the surface area of indentation should be the contact area while under the indentation force. As in-situ measurement of indentation diameter is not practical, the diameter is measured after removing the indenter. However, the indentation shape changes after removing the indentation force, primarily because of the elastic recovery of the test material. From FEA modeling, the indentation edge contact node point was determined at the maximum indentation force from model contact output and identified by the deformation geometry mesh. The corresponding mesh-node number and coordinate were identified, and by tracking the mesh contact node number, the position of the indentation edge contact point after removing the test force was determined.

### 5.2. Indentation contact pressure and surface stress distribution from FEA model

When an indentation force is applied to a spherical indenter, an indentation contact pressure is induced on the contact surface while no contact pressure is induced on the surface not in contact with the indenter. Figure 1 plots the normalized surface contact pressure, and the radial and circumferential stresses for typical pile-up and sink-in cases without friction. The  $x$ -axis is the indentation profile radial coordinate  $r$  normalized by the contact radius  $a_c$ . The  $y$ -axes are the (a) contact pressure  $P(r)$ , (b) radial stress  $\sigma_r(r)$  and (c) circumferential stress  $\sigma_\theta(r)$  along the indentation profile normalized with respect to the contact pressure at the indentation center  $P(0)$ . It can be seen from Figure 1(a) that the contact pressure increases from  $P(0)$  at the center of the indentation ( $r = 0$ ) to the maximum  $P(r)$  at  $r/a_c \cong 0.9$  and then smoothly drops to the normalized pressure of 0.8 at the normalized radius near the contact edge for the sink-in case; while, for the pile-up case, the contact pressure is maximized at the center, smoothly decreases along the contact radius until  $r/a_c \cong 0.95$ , then increases slightly and drops again. For both cases, the contact pressure around the contact edge shows a quick sharp drop from a normalized value of over 0.6 to zero. As both cases are modeled as having a frictionless interface between the indenter and specimen, the contact pressure is one of the principal stresses on the surface. The remaining two stress components of radial (see Figure 1(b) and circumferential (see Figure 1(c)) stress exhibited a sharp transition at the contact edge region as well. Within the contact area, both radial and circumferential stresses are compressive (lower than zero). Outside the contact region, the radial stress shifts to tension for the sink-in case while remaining as compression after a sharp increment at the contact edge for the pile-up case (see Figure 1(b)); the circumferential stresses showed tension for the sink-in case while changing from compression to tension and back to compression again at the contact edge for the pile-up case (see Figure 1(c)).

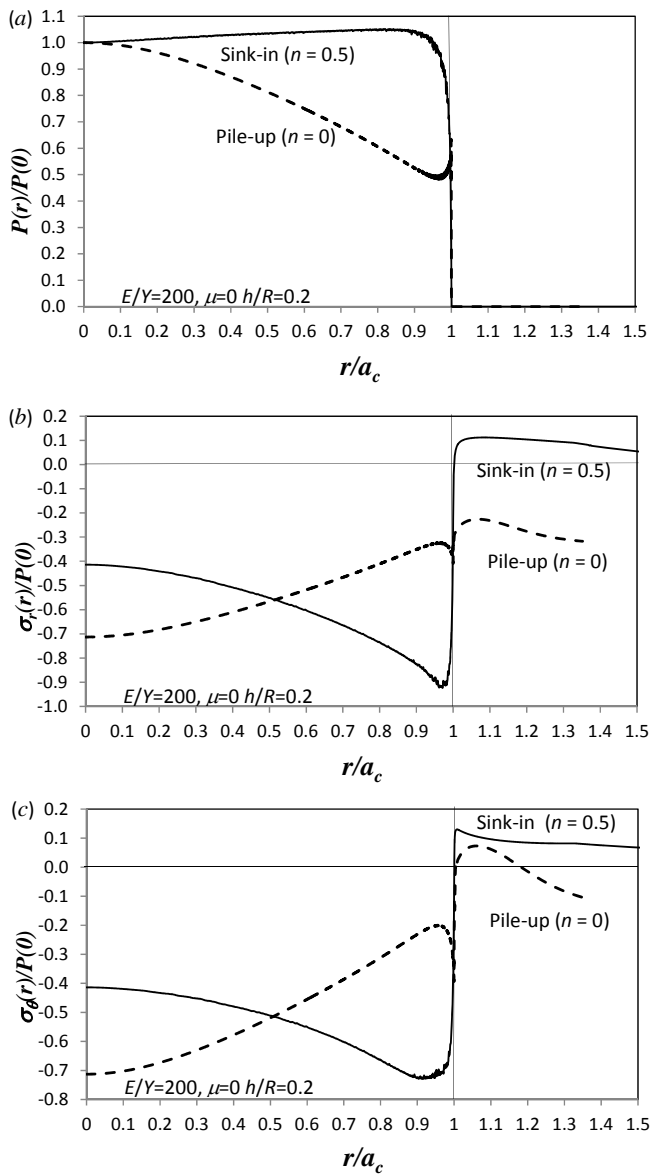


Figure 1. Normalized surface contact pressure (a), radial stress (b) and circumferential stress (c) distributions for pile-up and sink-in cases.

### 5.3. Indentation edge contact characteristics

From Figure 1, it can be seen that all of the surface pressure and stresses exhibit sharp changes at the contact edge. Those sharp changes should generate corresponding sharp deformation changes between the contact and non-contact regions at the edge of the indentation profile. Therefore, a sharp deformation change should occur at the contact edge. We define the slope angle  $\beta$  along the indentation profile as

$$\beta(r) = \tan^{-1} \left( \frac{\partial z}{\partial r} \right) \quad (2)$$

where  $r$  and  $z$  are the indentation profile radial coordinate and depth coordinate, respectively. For a digitized indentation profile, the slope angle can be calculated from point to point on the indentation profile as

$$\beta_i = \tan^{-1} \left( \frac{z_{i+1} - z_{i-1}}{r_{i+1} - r_{i-1}} \right) \quad (3)$$

where  $i$  represents the data point number. We also defined the change of slope angle, or slope rate,  $\beta'$ , as

$$\beta'(r) = \frac{\partial \beta}{\partial r} \quad (4)$$

which can be digitalized as

$$\beta'_i = \frac{\beta_{i+1} - \beta_{i-1}}{r_{i+1} - r_{i-1}} \quad (5)$$

The types of materials for which pile-up or sink-in occurs have been examined by finite element simulation by analyzing load and depth sensing indentation data. In general, pile-up is greatest in materials with large  $E/Y$  and little or no capacity for work hardening (i.e., “soft” metals that have been cold-worked prior to indentation). The ability to work-harden inhibits pile-up because as material at the surface adjacent to the indenter hardens during deformation, it constrains the upward flow of material to the surface. Sink-in predominates for materials with a work hardening value of  $n = 0.5$ . The cross-over from sink-in to pile-up should occur at  $n = 0.22$  [5]. The ratio of the elastic modulus to yield stress,  $E/Y$ , represents the relative amounts of elastic and plastic deformation. This parameter physically represents the reciprocal of the elastic strain at yielding and can therefore be used as a measure of the amount of deformation that is accommodated elastically during indentation. In the limit  $E/Y = 0$ , contact is strictly elastic and dominated by sink-in from Hertzian contact theory. At the other extreme, the limit  $E/Y = \infty$  corresponds to rigid-plastic deformation or  $n = 0$ , for which there is extensive pile-up of material around the hardness impression.

In this research, we selected strain hardening values of  $n = 0, 0.22$  and  $0.5$  for studying the pile-up, intermediate and sink-in cases. Figure 2 shows the normalized indentation profile  $z/b$  (Figure 2(a) and Figure 2(b)), its corresponding slope angle  $\beta$  (Figure 2(c) and Figure 2(d)) and the slope angle rate  $\beta'$  profiles (Figure 2(e) and Figure 2(f)) as a function of relative radius  $r/a$  ( $a$  is the surface contact radius at the maximum test force) while under the test force (left column) and after removing the test force (right column) for the pile-up ( $n = 0$ ) and sink-in ( $n = 0.5$ ) cases and an additional intermediate case ( $n = 0.22$ ) from FEA modeling. In all the cases,  $E/Y$  is 200 and the normalized indentation depth  $h/R$  is 0.2 at the maximum force. The crosses “ $\times$ ” in the figures indicate the indentation edge contact position. It can be seen that a typical curvature transition occurs at the contact edge region of the indentation profile while under the test force (see Figure 2(a)) and after removing the test force (see Figure 2(b)). However this transition point is not easily identified from the indentation profile. When we look at the slope angle profiles, the transition area stands out as a sharp slope angle change. Under the test force as shown in Figure 2(c), the slope angle increases from zero at the center of the indentation to the maximum near the contact edge and then drops sharply.

The contact edge coincides with the highest slope angle drop. After removing the load, due to the elastic recovery which is unevenly distributed along the radial direction, the slope angle shows an increase curve to maximum and drop again. The contact edge point is still at the maximum slope angle change. To make the contact edge position clearer, we plotted the slope rate profiles as shown in Figure 2(e) and Figure 2(f). The slope rate maintains almost no change across the entire indentation cross-section except an obvious narrow downward spike at the contact boundary region. The contact boundary was determined to be at the negative peak of the slope rate function both under the test force and after removing the test force.

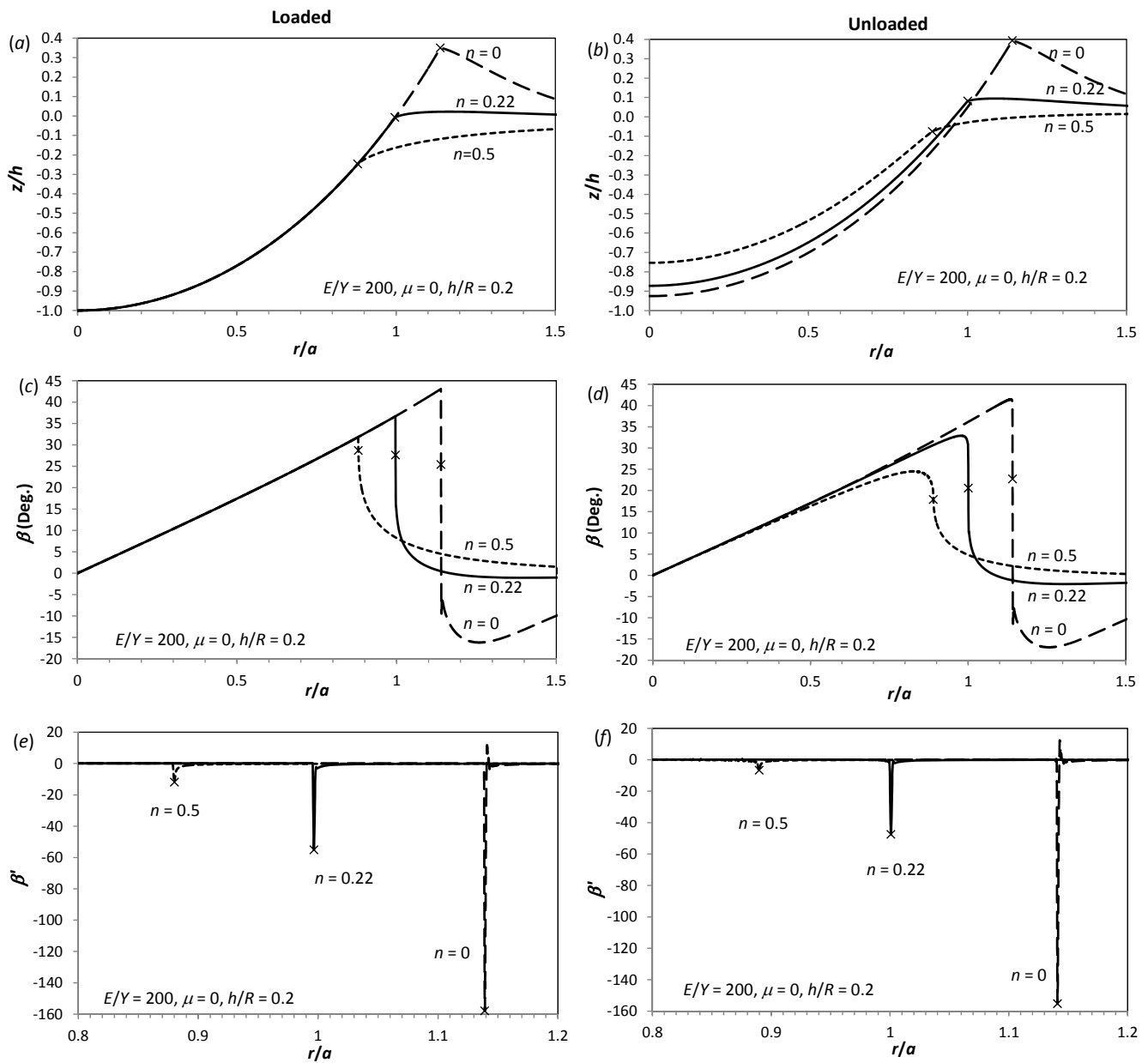


Figure 2. The indentation profile (a and b), its corresponding slope angle profile (c and d) and slope rate profile (e and f) on the test load and after removing the load for the pile-up ( $n = 0$ ), sunk-in ( $n = 0.5$ ) in Figure 1 and an additional intermediate ( $n = 0.22$ ) cases.

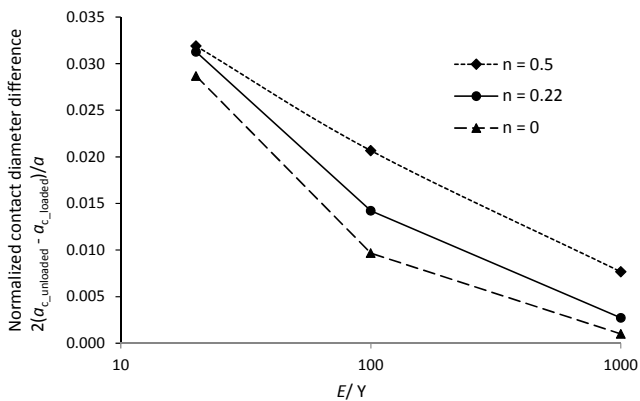


Figure 3. Normalized contact diameter difference between the loaded and unloaded conditions as a function of modulus yield stress ratio ( $E/Y$ ) for the materials with strain hardening  $n$  of 0, 0.22 and 0.5 under a normalized indentation depth of  $h/R = 0.2$ .

Figure 3 shows the normalized contact diameter difference between the loaded and unloaded conditions as a function of modulus yield stress ratio ( $E/Y$ ) for the pile-up/sink-in and intermediate cases under a normalized indentation depth of  $h/R = 0.2$ . It can be seen that the contact diameters enlarged after removing the indentation force because of the elastic recovery of the indented materials. Since the smaller  $E/Y$  represents a larger reciprocal of the elastic strain after plastic deformation, the increase in contact radius is larger on the  $E/Y = 20$  materials. As higher strain hardening contributes to a larger elastic strain ratio, there is a larger increase in the contact radius for higher strain hardening materials. The incremental increase in contact diameter  $2a_c$  relative to the surface contact radius  $2a$ , after removing the indentation force, decreases from 3.2% to 0.77% for the high strain hardening materials ( $n = 0.5$ ) and decreases from 2.8% to 0.1% for the materials without strain hardening ( $n = 0$ ) when  $E/Y$  increases from 20 to 1000.

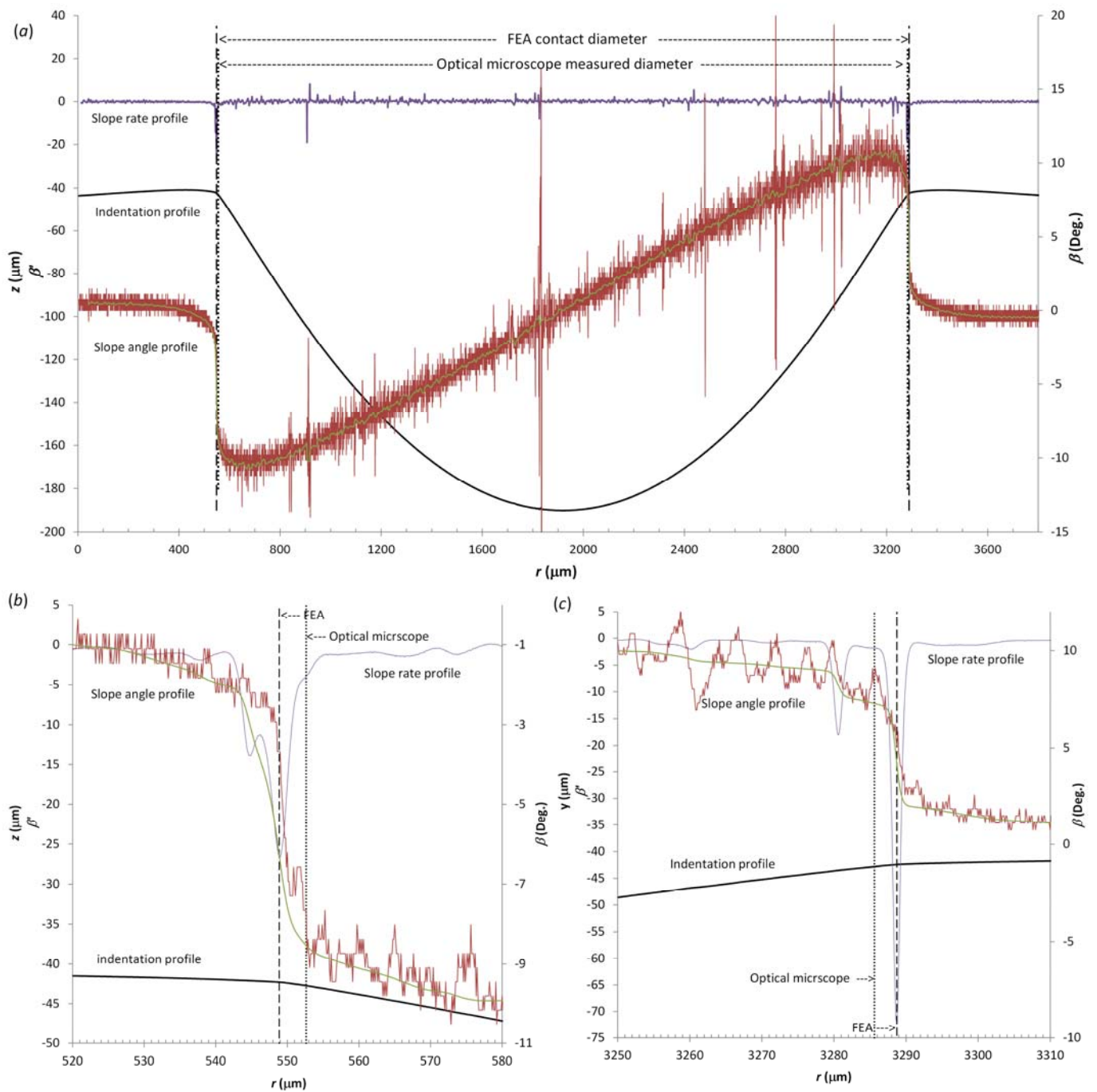


Figure 4. (a) Experimental indentation profile (black), its slope angle (red), filtered slope angle (green) and filtered change of slope angle profile (purple) with the FEA and optical microscope measured position; (b) left hand side detail and (c) right hand side detail of (a).

#### 5.4. A new method to determine the contact diameter from direct measurement

To verify that the above technique can be applied to real Brinell indentations, indentation experiments were done. The characteristics of the indentation profiles, the slope angle and slope angle rate profiles as measured with the profilometer display the same characteristics as the FEA model although with considerable more noise on the slope angle and slope rate profile results due to surface roughness.

From the above FEA study in Section 5.3, it can be seen that the trend in the position of the ball indentation contact boundary is consistent as the maximum slope angle  $\beta$  change or the negative peak of slope rate  $\beta'$  profile for various indentation

materials and conditions. This is most obvious on the slope rate profile. Therefore, we suggest a new method to determine the contact diameter from direct measurement of the surface profile of the diametrical cross-section of the Brinell indentation. The slope angle  $\beta$  and slope rate  $\beta'$  profiles are calculated from the indentation profile using Eq.3 and 5 from which the indentation contact boundary position may be determined from the negative peak of the slope rate. The indentation diameter based on the contact boundary positions can then be calculated.

Applying this new method, we measured several experimental Brinell indentation profiles and calculated diameters using this technique. Figure 4 demonstrates an experimental indentation made in a 503 HBW 10/3000 material

using a 10 mm diameter ball and 29,420 N (3000 kgf) applied force. The indentation profile was measured using a stylus profilometer instrument. Its slope angle profile was calculated by Eq. 3. To minimize the effect of measurement noise due to surface roughness of the indented material on the slope angle and slope rate determinations, a Gaussian filter with an 8  $\mu\text{m}$  short cutoff was applied to the slope angle profile. The slope rate profile is based on the filtered slope angle profile. The indentation contact diameter position was chosen using our new method as shown in Figure 4 dashed line. Meanwhile, the indentation diameter was measured using the optical measuring system by a secondary calibration laboratory. The indentation boundary location was picked from the actual measured diameter value, which is also indicated in Figure 4 as a dotted line. It can be seen that the locations of the edge of the indentation measured using our suggested method and using the optical measuring microscope are not the same. The optical measuring microscope measured the indentation diameter about 7  $\mu\text{m}$  smaller than the actual contact diameter, corresponding to a 2.6 HBW difference.

## 6. CONCLUSIONS

The Brinell indentation diameter was investigated using FEA modeling of indentations on various indentation pile-up and sink-in conditions, including materials' strain hardening and the ratio of Young's modulus to yield stress. The surface contact pressure and stress distribution exhibit sharp changes at the contact region. Similarly, the indentation slope angle and slope rate profile show sharp changes at the contact region for various materials. For both the loaded and unloaded conditions, the contact edge point is always at the maximum slope angle change or the negative peak of the slope rate profile.

The contact diameters enlarged after removing the indentation force because of the elastic recovery of the indented materials. The contact diameter increment after removing the indentation load is larger for materials with higher strain hardening and lower ratio of Young's modulus to yield stress under deeper indentation with no friction.

A new method is proposed to determine the edge of a Brinell indentation from surface profile measurements. FEA modeling has shown that the indentation contact boundary can be determined after unloading from the negative peak of the slope rate profile. By applying this method to real Brinell indentations, this method provides an effective way for the national metrology institutes to obtain the indentation diameter for various materials and indentation conditions without the biases of optical measurements and an undefined indentation edge. This should improve the agreement on the calibrated Brinell indentation reference among the national metrology

institutes, and therefore increase the agreement propagated down to the users.

## ACKNOWLEDGEMENT

The authors are grateful to Brian Renegar for the valuable profilometer scan indentation measurements.

## REFERENCES

- [1] H. Chardler, *Hardness Testing*. ASM International, 1999.
- [2] D. Tabor, *Hardness of Metals*: Oxford: Clarendon Press, 1951.
- [3] H. O'Neill, *Hardness Measurement of Metals and Alloys*: Chapman and Hall Ltd., 11 new fether Lane, London EC4, 1967.
- [4] J.R. Matthews, Indentation hardness and hot pressing, *Acta Metallurgica* 28 (1979) pp. 311-318.
- [5] R. Hill, B. Storakers, A.B. Zdunek, A Theoretical Study of the Brinell Hardness Test, *Proceedings of the Royal Society of London. Series A, Mathematical and Physical Sciences* 423 (1989) pp.301-330.
- [6] J, Alcalá, A.C. Barone, M. Anglada, The influence of plastic hardening on surface deformation modes around Vickers and spherical indents, *Acta Materialia* 48 (2000) pp.451-3464.
- [7] K, Ai, L. Dai, Numerical study of pile-up in bulk metallic glass during spherical indentation, *Science in China Series G: Physics Mechanics and Astronomy* 51 (2008) pp.379-386.
- [8] S.H. Kim, B.W. Lee, Y. Choi, D. Kwon, Quantitative determination of contact depth during spherical indentation of metallic materials - A FEM study, *Materials Science and Engineering A-Structural Materials Properties Microstructure and Processing* 415 (2006) pp.59-65.
- [9] Y.T. Cheng, C.M. Cheng, Effects of 'sinking in' and 'piling up' on estimating the contact area under load in indentation, *Philosophical Magazine Letters* 78 (1998) pp.115-120.
- [10] H. Habbab, B.G. Mellor, S. Syngellakis, Post-yield characterisation of metals with significant pile-up through spherical indentations, *Acta Materialia* 54 (2006) pp.1965-1973.
- [11] G. Barbato and S. Desogus, Problems in the Measurement of Vickers and Brinell Undentations, *Measurement* 4 (1986) pp.137-147.
- [12] A. Germak, K. Herrmann, and S. Low, Traceability in Hardness Measurements: from the Definition to Industry, *Metrologia*, 47 (2010) S59-S66.
- [13] L. Ma, S. Low, and J. Song, "Investigation of Brinell indentation diameter from confocal microscope measurement and FEA modeling", In *Proc. of HARDMEKO 2007*, Nov. 19-21, 2007, Tsukuba, Japan.
- [14] Standard Test Method for Brinell Hardness of Metallic Materials. [E10-01]. American Society of Testing and Methods, 2001.
- [15] ISO 6506-1:2005, *Metallic materials-Brinell hardness test – Part 1: Test method*. Geneve, Switzerland: International Organization for Standardization, 2005.
- [16] B. Taljat, G.M. Pharr, Development of pile-up during spherical indentation of elastic-plastic solids, *International Journal of Solids and Structures* 41 (2004) pp.3891-3904.